Journal of Physics: Conference Series **2767** (2024) 032050 doi:10.1088/1742-6596/2767/3/032050

Controller design for the X-Rotor offshore wind turbine concept

L Recalde-Camacho, W Leithead, L Morgan and A Kazemi Amiri

Wind Energy and Control Centre, Department of Electronic and Electrical Engineering, University of Strathclyde, Glasgow G1 1XW, UK

E-mail: luis.recalde-camacho@strath.ac.uk

Abstract. This paper explores the design of a full envelope speed controller to operate the X-Rotor Offshore Wind Turbine. The X-Rotor is a heavily modified V-rotor vertical axis wind turbine, in which the primary rotor has conventional blades angled both up and down from the ends of a relatively short and stiff cross-arm. The upper half employs full span blade pitching for speed regulation and the lower half is aimed at reducing overturning moments on the main bearing and provides power take-off through compact secondary horizontal axis turbines mounted at the tip of the lower blades. The operational strategy is somewhat similar to that of a variable speed pitch regulated horizontal axis wind turbine, however it differs in the following aspects: the way aerodynamic torque is balanced across the operating envelope, the adjustment of equilibrium operating points at below rated operation, the relationship of aerodynamic torque on the primary rotor to pitch angle, and the operation of the secondary rotors to increase energy capture. These aspects increase the complexity of the control strategy but also ease the controller requirements. The developed controller is tested on a turbine model with sufficient complexity to model the essential dynamic properties of the turbine concept.

1. Introduction

The X-Rotor is a multi-megawatt vertical axis wind turbine (VAWT) concept aimed at large scale offshore commercial deployment. Compared to horizontal axis wind turbines (HAWT), early developments in VAWT showed two fundamental design challenges, the aerodynamic efficiency is intrinsically lower, requiring the VAWT to be 15% to 20% larger than a HAWT to produce the same power, and the optimum speed is less than half of a comparable HAWT, thus leading to the use of drive-trains twice as heavy and expensive [1]. Previous VAWT technologies worth mention are the "V" type VAWT, largely developed in UK University R&D by David Sharpe and co-workers, and the NOVA design which took the V design a stage further by improving the low aerodynamic efficiency, but led to major problems for the drive-train weight and cost. The X-Rotor concept is a heavily modified V-VAWT. The primary rotor of the X-Rotor has conventional blades angled both up and down from the ends of a relatively short and stiff cross-arm. The upper half of the X-rotor employs full span blade pitching to improve rotor efficiency, energy capture and provides speed control, active damping of blade and rotor vibrations and rotor overspeed protection in various fault case scenarios. The lower half is aimed at reducing overturning moments on the main bearing and provides power take-off through compact secondary horizontal axis turbines mounted at the tip of the lower blades. Early feasibility study of the X-rotor concept, carried out in [1], has shown potential to reduce

the Cost of Energy (CoE) by up to 26% as compared to four existing wind turbine types. In [2], the O&M cost modelling of novel offshore wind turbine concepts, including the X-Rotor, is presented. in [3], a modified O&M cost model that facilitates the modelling of X-Rotor systems is developed. Such studies facilitate the comparison of O&M cost of an X-Rotor against a conventional HAWT of equal power rating and found that the X-Rotor could introduce savings between 20% and 40%. In [4], the development and validation of a double streamtube model to model the X-Rotor primary rotor is presented. The study demonstrated that the primary rotor could achieve power coefficients up to 0.45, which is 10% larger than the value considered in the feasibility study from [1]. Experimental studies of the near wake of the X-Rotor have also been carried out in [5], and showed a clear impact on the streamwise and axial induction fields as well as the local presence of vorticity structures.

This paper explores the operation of the X-Rotor by developing both a suitable control strategy and the controllers required. The operational strategy is somewhat similar to that of a variable speed pitch regulated HAWT to allow a fair comparison. However, the are some aspects where the X-Rotor concept which are somewhat different and need to be addressed before selecting a control strategy. First, the aerodynamic torque on the primary rotor is not balanced by the reaction torque from the generator, instead it is balanced by the thrust of the secondary rotors. Second, in below rated operation, the turbine is regulated by changing the rotor speed and thrust of the secondary rotors and the equilibrium operating points are stable since the ratio of the thrust of the secondary rotor to the torque of the primary rotor is constant irrespective of wind speed, when both rotors track its maximum tip speed ratio. Third, the primary rotor operates at its maximum aerodynamic efficiency up to rated wind speed, at which point pitching commences. To maintain constant power of the primary rotor, a very rapid change in pitch is required, follow by a slow pitch change. Change in pitch angle can be either positive or negative, however in this study negative pitching schedule is selected as thrust is reduced during the upstream sweep when the blades are pitched away from feather and the aerodynamic efficiency of the turbine is closed to that of a HAWT [6]. Fourth, each secondary rotor experiences a sinusoidal varying wind speed as it rotates periodically into and out of the ambient wind speed. This causes an energy capture increase of approximately $100\,(V_P/V_S)^2\,\%$ when the rotors operate at constant tip speed ratio. V_P is the ambient wind speed experienced by the primary rotor and V_S is the incident wind speed experienced by the secondary rotors.

Traditionally, at below rated operation, VAWTs are made to track their maximum aerodynamic efficiency, whereas at above rated wind speeds power is regulated and smoothed. Both passive and active dynamic stall control, and blade pitch control have been used, at above rated operation, to mitigate flow separation and delay stall at low tip speed ratios. Reviews of both control methods can be found in [7] and [8], respectively. The use of pitch control is further restricted for VAWTs due to the continues changes in both the relative wind speed and the angle of attack of the blade. However, as demonstrated in [6] the X-Rotor shows a high performance coefficient, similar to that of a HAWT and eases the application of conventional pitch control. the control task and therefore the controllers required to regulate the operation of the primary rotor and the HAWT secondary rotors are rather simpler than the required control strategy.

The rest of the paper is organised as follows. In Section 2 an azimuth-independent model of the X-Rotor is presented. The model is linearised and used for system analysis and controller development. The control strategy required for full envelope operation is described. The four modes of operation required are detailed and its control requirements are defined. In Section 3, the required controllers are designed and the system frequency response is presented to show the stability margins of the designed control systems. Simulation studies are shown in Section 4. The developed control strategy and its corresponding controllers are tested on an azimuth-dependent full nonlinear model of the X-Rotor implemented in Simulink. The effective wind-field model, developed in [9], is used for the simulations studies. Finally in Section 5 conclusions are drawn.

2. Turbine Model and Operation

2.1. X-rotor Model for Control

The dynamic structure of the X-rotor is presented in Figure 1, where subscripts $_P$ and $_S$ represent primary and secondary rotor variables respectively. At the primary rotor, β is the pitch angle of the upper blades and Ω_P is rotor speed. At the secondary rotor, k_c is the rotor gain to track some specific tip speed ratio λ_S, Ω_S is the rotor speed and T_S is the thrust force.

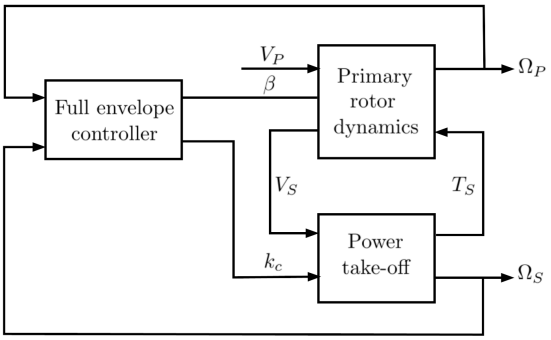

Figure 1: X-Rotor dynamic structure and controller

Aerodynamically, the secondary rotor experiences an incident wind speed, which varies with azimuth angle, θ; and exerts a thrust force, which balances the aerodynamic torque, Q_P, on the primary rotor, that is

$$V_S = \Omega_P R_P + V_P \sin(\theta) \tag{1}$$

$$\underbrace{\left[\frac{1}{\Omega_P}\frac{1}{2}\rho A_P C_{P_P}(\lambda_P, \beta) V_P^3\right]}_{\overline{Q_P}} = N R_P \underbrace{\left[\frac{1}{2}\rho A_S \overline{C_{T_S}(\lambda_S, \theta) V_S^2}\right]}_{\overline{T_S}} \tag{2}$$

Here, the overline $\overline{(\cdot)}$ denotes variables averaged over a primary rotor revolution. A_P and A_S are the primary and secondary rotor areas, respectively, R_P is the primary rotor radius, N is the number of secondary rotors, C_{P_P} is the primary rotor power coefficient and C_{T_S} is the secondary rotor thrust coefficient. The primary and secondary rotors tip speed ratios are given by $\lambda_P = \frac{\Omega_P R_P}{V_P}; \lambda_S = \frac{\Omega_S R_S}{V_S}$, respectively. The primary rotor aerodynamics are obtained using a double multiple streamtube (DMS) model and validated against the higher fidelity CACTUS lifting line model, whereas the secondary rotors are modelled using an actuator disc model, validated against the BEM tool QBlade. Validation results can be found in [9].

The turbine aerodynamics presented in Equation 2 can be used to determine the aerodynamic efficiency of power conversion between the primary and secondary rotors as the ratio between the revolution averaged power from the secondary rotor to the captured power by the primary rotor. While the rotors operate at constant tip speed ratio, this is given by:

$$\eta \approx \frac{\overline{C_{P_S}(\lambda_S, \theta)}}{\overline{C_{T_S}(\lambda_S, \theta)}} \left(\frac{1 + \frac{3}{2}\lambda_P^{-2}}{1 + \frac{1}{2}\lambda_P^{-2}}\right). \tag{3}$$

and the full rotor power coefficient is therefore given by

$$C_P = C_{P_P}\eta \tag{4}$$

Structurally, the primary rotor model includes compliant upper blade dynamics represented by a single blade model whereby only the lowest tangential and normal dynamic modes are

included and pitch in unison. The blade modal analysis was presented in [1]. The cross-arm is considered rigid. and lower part includes semi-compliant lower blade dynamics which are considered to be rigid since they are much stiffer and flex much less than the upper blades. The power take-off is treated as an actuator with its bandwidth sufficiently large and its dynamics modelled as a semi-compliant shaft connected to a direct drive permanent magnet synchronous generator (PMSG). The electrical dynamics are also considered to be relatively high frequency. The azimuthal variation in V_S is neglected but its effect on the secondary rotor aerodynamic thrust and torque, averaged over azimuthal angle, is included. The resulting simplified model is nonlinear but does not retain any dependence on azimuth angle.

Relative to the equilibrium operating point, the turbine linearised dynamics are as follows.

$$(V_{P_0}, \beta_0, V_{S_0}, k_{c_0}, \theta_{P_0}, \phi_{P_0}, \Omega_{P_0}, \Phi_{P_0}, \theta_{H_0}, \Omega_{H_0}, M_{PA\theta_0}, M_{PA\phi_0}, T_{S_0}, \Omega_{G_0}, T_{RG_0}, \lambda_{S_0})$$

Upper rotor:

$$\begin{aligned}
&J_P \begin{bmatrix} \Delta\dot{\Omega}_P \\ \Delta\dot{\Phi}_P \end{bmatrix} = -J_P \begin{bmatrix} \left(\omega_e^2 c_{\beta_0}^2 + \omega_f^2 s_{\beta_0}^2\right) & -\left(\omega_e^2 - \omega_f^2\right) s_{\beta_0} c_{\beta_0} \\ -\left(\omega_e^2 - \omega_f^2\right) s_{\beta_0} c_{\beta_0} & \left(\omega_e^2 s_{\beta_0}^2 + \omega_f^2 c_{\beta_0}^2\right) \end{bmatrix} \begin{bmatrix} \Delta\theta_P - \Delta\theta_H \\ \Delta\phi_P \end{bmatrix} \\
&- J_P \begin{bmatrix} \left(\gamma_e^2 c_{\beta_0}^2 + \gamma_f^2 s_{\beta_0}^2\right) & -\left(\gamma_e^2 - \gamma_f^2\right) s_{\beta_0} c_{\beta_0} \\ -\left(\gamma_e^2 - \gamma_f^2\right) s_{\beta_0} c_{\beta_0} & \left(\gamma_e^2 s_{\beta_0}^2 + \gamma_f^2 c_{\beta_0}^2\right) \end{bmatrix} \begin{bmatrix} \Delta\Omega_P - \Delta\Omega_H \\ \Delta\Phi_P \end{bmatrix} \\
&- J_P \begin{bmatrix} -\sin(2\beta_0) & -\cos(2\beta_0) \\ -\cos(2\beta_0) & -\sin(2\beta_0) \end{bmatrix} \left\{ \left(\omega_e^2 - \omega_f^2\right) \begin{bmatrix} \theta_{P_0} - \theta_{H_0} \\ \phi_{P_0} - \psi \end{bmatrix} + \left(\gamma_e^2 - \gamma_f^2\right) \begin{bmatrix} \Omega_{P_0} - \Omega_{H_0} \\ \Phi_{P_0} \end{bmatrix} \right\} \Delta\beta \\
&+ \begin{bmatrix} \frac{\partial M_{PA\theta}}{\partial \Omega_P} \\ \frac{\partial M_{PA\phi}}{\partial \Omega_P} \end{bmatrix} \Delta\Omega_P + \begin{bmatrix} \frac{\partial M_{PA\theta}}{\partial \beta} \\ \frac{\partial M_{PA\phi}}{\partial \beta} \end{bmatrix} \Delta\beta + \begin{bmatrix} \frac{\partial M_{PA\theta}}{\partial V_P} \\ \frac{\partial M_{PA\phi}}{\partial V_P} \end{bmatrix} \Delta V_P \\
&+ \begin{bmatrix} 0 \\ -\left(J_P + \tilde{J}_P\right) \Omega_{H_0}^2 \sin(\phi_{P_0}) + g M_P l_{P_{cm}} \cos(\phi_{P_0}) \end{bmatrix} \Delta\phi_P \\
&+ \begin{bmatrix} 0 \\ -\left(J_P + \tilde{J}_P\right) 2\Omega_{H_0}^2 \cos(\phi_{P_0}) \end{bmatrix} \Delta\Omega_P
\end{aligned} \tag{5}$$

$$\begin{bmatrix} \Delta\dot{\theta}_P \\ \Delta\dot{\phi}_P \end{bmatrix} = \begin{bmatrix} \Delta\Omega_P \\ \Delta\Phi_P \end{bmatrix} \tag{6}$$

Cross-arm:

$$J_H \Delta\dot{\Omega}_H = \Delta Q_{P_U} + \Delta Q_{P_L} - R_P \Delta T_S \tag{7}$$

$$\Delta\dot{\theta}_H = \Delta\Omega_H \tag{8}$$

$$\begin{aligned}
\Delta Q_P &= J_P \begin{bmatrix} \left(\omega_e^2 c_{\beta_0}^2 + \omega_f^2 s_{\beta_0}^2\right) & -\left(\omega_e^2 - \omega_f^2\right) s_{\beta_0} c_{\beta_0} \end{bmatrix} \begin{bmatrix} \Delta\theta_P - \Delta\theta_H \\ \Delta\phi_P \end{bmatrix} \\
&+ J_P \begin{bmatrix} \left(\gamma_e^2 c_{\beta_0}^2 + \gamma_f^2 s_{\beta_0}^2\right) & -\left(\gamma_e^2 - \gamma_f^2\right) s_{\beta_0} c_{\beta_0} \end{bmatrix} \begin{bmatrix} \Delta\Omega_P - \Delta\Omega_H \\ \Delta\Phi_P \end{bmatrix} \\
&+ J_P \begin{bmatrix} -\sin(2\beta_0) & -\cos(2\beta_0) \end{bmatrix} \left\{ \left(\omega_e^2 - \omega_f^2\right) \begin{bmatrix} \theta_{P_0} - \theta_{H_0} \\ \phi_{P_0} - \psi \end{bmatrix} + \left(\gamma_e^2 - \gamma_f^2\right) \begin{bmatrix} \Omega_{P_0} - \Omega_{H_0} \\ \Phi_{P_0} \end{bmatrix} \right\} \Delta\beta
\end{aligned} \tag{9}$$

$$\Delta Q_{P_L} = \frac{\delta M_{PAL\theta}}{\delta \Omega_H} \Delta\Omega_H + \frac{\delta M_{PAL\theta}}{\delta V_P} \Delta V_P \tag{10}$$

Power take-off:

$$J_S \Delta\dot{\Omega}_S = \Delta Q_S - \Delta Q_{RG} \tag{11}$$

$$\Delta\dot{Q}_{RG} = K_S \left(\Delta\Omega_S - \Delta\Omega_G\right) \tag{12}$$

$$J_G \Delta\dot{\Omega}_G = \Delta Q_{RG} - 2k_{c_0} - 2k_{c_0}\Omega_{S_0}\Delta\Omega_S - \Omega_{G_0}^2 \Delta k_c \tag{13}$$

$$\Delta Q_S = \frac{\partial Q_S}{\partial \Omega_S}\Delta\Omega_S + \frac{\partial Q_S}{\partial \Omega_P}\Delta k_c; \Delta T_S = \frac{\partial T_S}{\partial \Omega_S}\Delta\Omega_S + \frac{\partial T_S}{\partial \Omega_P}\Delta k_c \tag{14}$$

where s_{β_0} and c_{β_0} are short notations for $\sin(\beta_0)$ and $\cos(\beta_0)$.

The used variables are: tangential, θ_P, and normal, ϕ_P, angular displacements of the upper blades, angular displacement of the cross-arm, θ_H, coning angle of the upper blade, ψ, aerodynamic torque from the upper, Q_{P_U} and lower, Q_{P_L} primary rotor blades, shaft torque, Q_{RG}, secondary rotor torque, Q_S, and generator speed, Ω_G. Additionally, the turbine parameters are: primary, J_P, secondary, J_S, cross-arm, J_H and generator, J_G, inertias; tangential, ω_e, and normal, ω_f, frequencies of the upper blades; tangential, γ_e, and normal, γ_f, damping coefficients of the upper blades; tnagential, $M_{PA\theta}$, and normal, $M_{PA\phi}$, aerodynamic blade bending moments for the upper blades; tangential aerodynamic blade bending moment of the lower blades, $M_{PAL\theta}$, mass of the upper blades, M_P, distance between the upper blade centre of mass and its root, $l_{P_{cm}}$, gravity, g and

$$\tilde{J}_P = M_P\left(l_c^2 + 2l_c l_{P_{cm}}\sin(\phi_P) - l_c^2\sin^2(\phi_P)\right) \tag{15}$$

These linearised dynamics suffice when the bandwidth of the power take-off are sufficiently large and can be used to design suitable speed controllers.

2.2. Overview of the turbine operational strategy

In the torque/rotor speed plane, the operational strategy for the X-rotor encompasses 4 modes of operation: constant secondary rotor speed (mode 1), $C_{P_{\max}}$ tracking (mode 2), pre-emptive pitching (mode 3), and constant torque and rotor speed (mode 4). To average out the sinusoidal variations of rotor speed during one rotation, the rotational speed of both secondary rotors is averaged as follows:

$$\bar{\Omega}_s = \frac{1}{2}\left(\Omega_{s_1} + \Omega_{s_2}\right) \tag{16}$$

In mode 1, at very low wind speeds, just above cut-in, $\bar{\Omega}_s$ is held constant by adjusting λ_s, for each rotor, through k_c. A minimum secondary rotor speed is imposed by the minimum AC output frequency of the PMSG and is given by $\bar{\Omega}_{s_{\min}} = \frac{2\pi}{n_p} f_{\min}$, where n_p is the number of pole pairs in the generator.

The secondary rotor output is

$$y_S = \bar{\Omega}_{S_{\min}} - \bar{\Omega}_S \tag{17}$$

A suitable controller can be designed to reduce the steady state error of the output. The rotational speed of the primary rotor is reduced to reduce induced wind speed, and thereby the secondary rotor thrust, which causes a reduction in the primary rotor torque to keep the balance.

In mode 2, at intermediate wind speeds, energy capture is maximised by operating both the primary and secondary rotors at their maximum aerodynamic efficiency, $C_{P_S}(\lambda_{S_{\max}}, 0)$, that is $k_c = k_{\text{opt}}$, where k_{opt} is constant. Using Equation 2, the required secondary rotor area to operate at maximum aerodynamic efficiency is given by

$$A_S = \frac{A_P C_{P_P}(\lambda_{P_{\max}}, 0)}{N\left(\lambda_{P_{\max}}^3 + \frac{1}{2}\lambda_{P_{\max}}\right) C_{T_S}(\lambda_{S_{\max}})} \tag{18}$$

For sufficiently high frequency electrical dynamics, the secondary rotors output reduces to

$$y_S = Q_{RC} - k_c \Omega_G^2 \tag{19}$$

Introducing an estimate of the secondary rotor aerodynamic torque, to directly track the $C_{P_{\max}}$ curve, to decrease the off-design energy discrepancy, leads to the following output

$$y_S = \hat{Q}_S - k_c \Omega_G^2 \tag{20}$$

where $\hat{Q}_S = J\hat{\Omega}_d + B\Omega_S + Q_{RG}$, with $\hat{\Omega}_d$ being an estimate of the secondary rotor acceleration given by

$$\hat{\Omega}_d = \frac{as}{s+a}\Omega_S \tag{21}$$

Here, J is the sum of all inertias in the drive-train, $J = J_S + J_G$, and B is the drive-train damping due to losses. The corner frequency, a, of the low pass filter is chosen to reduce the level of noise without introducing too much lag [10].

Therefore, the secondary rotor output becomes

$$y_S = Q_{RC} + H(s)\bar{\Omega}_S - k_c \Omega_G^2 \tag{22}$$

where $H(s)$ is a transfer function linearly related to $\bar{\Omega}_s$. Keeping k_c fixed ensures the tip speed ratio of the primary rotor is also constant, through the balancing torque, and tracks its $C_{P_P}(\lambda_{P_{\max}}, 0)$,

In mode 3, at wind speeds just below rated wind speed, pitch demand β_d of the upper blades is adjusted, as a function of primary rotor speed, to reduce pitch activity that otherwise would be very high at wind speeds just above rated, that is

$$\beta_d = f(\Omega_R) \tag{23}$$

Such pre-emptive pitching strategy reduces primary rotor torque, however the induced wind speed on the secondary rotors at any value remains unchanged and forces λ_S and consquently T_S to increase to balance Q_P. The secondary rotor output thus becomes

$$y_S = Q_{RC} + H(s)\bar{\Omega}_S - k_c(\Omega_P)\Omega_G^2 \tag{24}$$

In mode 4, at above rated wind speeds, the average thrust from the secondary rotors and the primary rotor speed are held constant by adjusting k_c and β_d, respectively. the turbine outputs are

$$y_P = \Omega_{P_{\text{rated}}} - \Omega_P \tag{25}$$

$$y_S = \bar{\Omega}_{S_{\text{rated}}} - \bar{\Omega}_S \tag{26}$$

The operational strategies for the primary and secondary rotors are shown in Figures 2 and 3, respectively. Figures 4 and 5 show the turbine power and the required pitch action from the blades of the primary rotor. [ht]

3. Full Envelope Controller Design

The full envelope controller for the X-Rotor comprises one tip speed ratio tracking controller that regulates the power take-off at below rated wind speed values, one pre-emptive pitch action to reduce pitch activity at values close to rated wind speed, and one pitch controller that regulates the operation of the primary rotor at above rated values. The tip speed ratio tracking controller continues to operate at above rated values but keeps the tip speed at a constant value and therefore does not require further control actions. Figures 6 and 7 show the frequency response

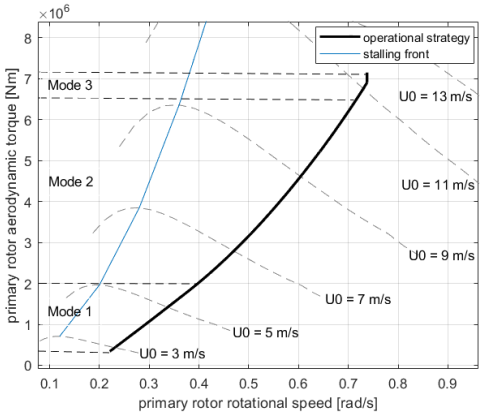

Figure 2: Primary rotor operating strategy

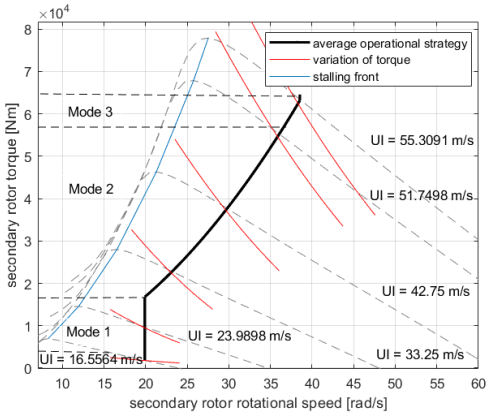

Figure 3: Secondary rotor operating strategy

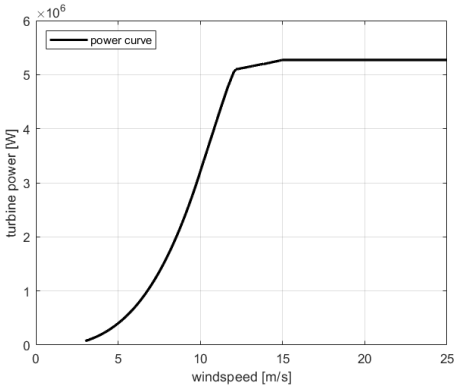

Figure 4: X-Rotor power curve

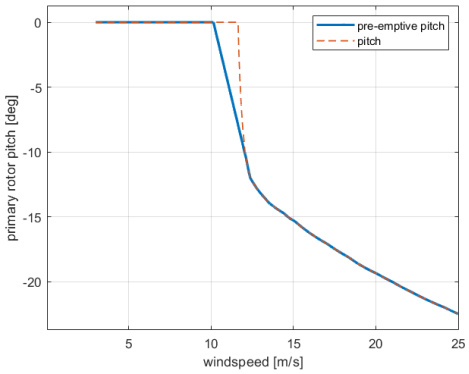

Figure 5: Primary rotor pitching strategy

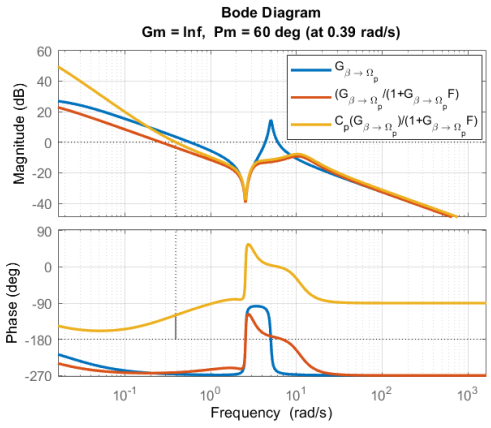

Figure 6: Controlled primary rotor frequency response

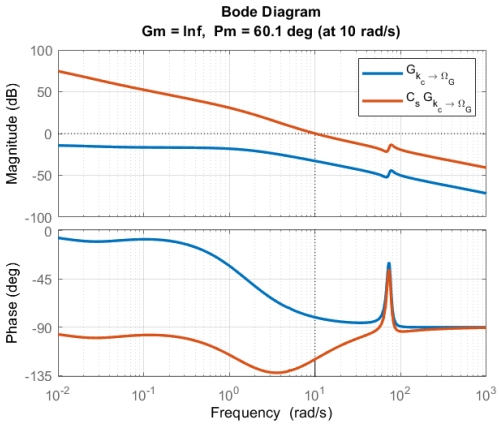

Figure 7: Controlled secondary rotor frequency response

of the transmittance from β to Ω_p for the primary rotor, $G_{\beta\to\Omega_P}$, and the transmittance from k_c to Ω_G for the secondary rotor, $G_{k_c\to\Omega_S}$, respectively. The primary rotor dynamics contain a resonant mode around the blade edgewise frequency. A feedback filter is designed to provide

active damping at such frequency mode. The filter dynamics are given by

$$F(s) = \frac{-40s}{(s+2.89)(s+6.503)} \tag{27}$$

The active damping is achieved by adding the filter in the feedback path and therefore acting on oncoming primary rotor speed measurements, that is

$$G_P = \frac{G_{\beta\to\Omega_P}(s)}{1 + G_{\beta\to\Omega_P}(s) F(s)} \tag{28}$$

In above rated wind speed values, the speed of the primary rotor is regulated by collective pitch control. As shown in Figure 5, the initial very rapid change in pitch angle is catered by the pre-emptive pitching strategy, therefore a slow PI controller suffices to regulate the relatively slow change in pitch. In this pitching schedule, the pitch angles are negative, that is, during the upstream sweep, the blades are pitched away from feather. The designed PI controller dynamics are

$$C_p(s) = \frac{1.1767(s+0.3s)}{s} \tag{29}$$

The combined PI controller and feedback filter achieves a phase margin of 60° at 0.39rad/s gain crossover frequency.

A linear pre-emptive pitching is designed to be

$$\beta_d = \frac{\Omega_P - \Omega_P(V_{P_1})}{\Omega_P(V_{P_2}) - \Omega_P(V_{P_1})} \tag{30}$$

where V_{P_2} and V_{P_1} represent the upper and lower bounds of the wind speed range around rated wind speed, and $\Omega_P(V_{P_2})$ and $\Omega_P(V_{P_1})$ are calculated during the design of the control strategy.

In below rated values, the secondary rotors are controlled by varying the electrical frequency given by the generators and the required power electronics are housed at the hub of the main rotor. When the secondary rotors require to keep a constant rotor speed, a simple PI controller can provide the required tip speed ratio. The secondary rotor controller dynamics are

$$C_s(s) = \frac{34.194(s+8.13)}{s} \tag{31}$$

The secondary rotor dynamics do not contain any resonant modes and the PI controller is tuned to achieve a phase margin of 60.1° at 10rad/s gain crossover frequency.

In above rated wind speed values, the secondary rotors are controlled to maintain revolution average rated power, thus the PI controller can be regulated the rotation variations in induced wind speed. The high bandwidth of the secondary rotor controller guarantees that both primary and secondary rotor controllers are completely decouple, particularly at above rated wind speed values when both controllers are active.

4. Simulation Results

The developed control strategy and controllers are tested on an azimuth-dependent full nonlinear model in Simulink. Effective wind speed field is set to have a turbulence intensity of 10%. The secondary rotor controller is active a below rated values between 3-6m/s wind speed. Figure 8 shows the secondary rotor speed and mechanical torque delivered by the controller. The sustained oscillation on the secondary rotor speed is due to 2p rotational sampling induced by the primary rotor. At 8m/s wind speed the turbine enters in mode 2 and the secondary rotor

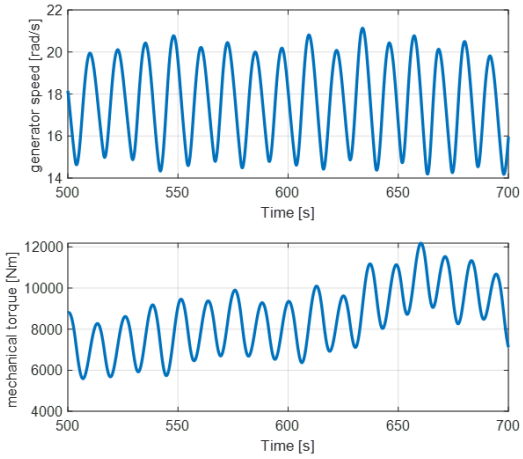

Figure 8: Secondary rotor speed and mechanical torque at 4m/s wind speed

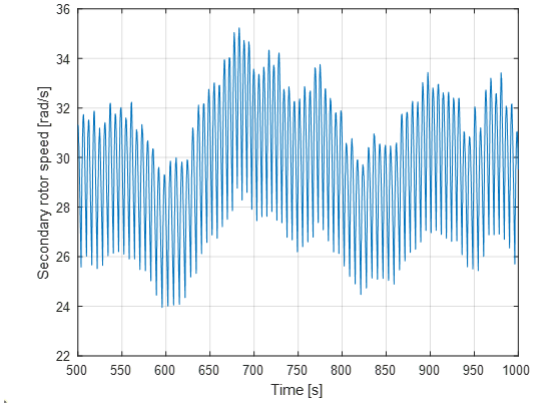

Figure 9: Secondary rotor speed at 8m/s wind speed

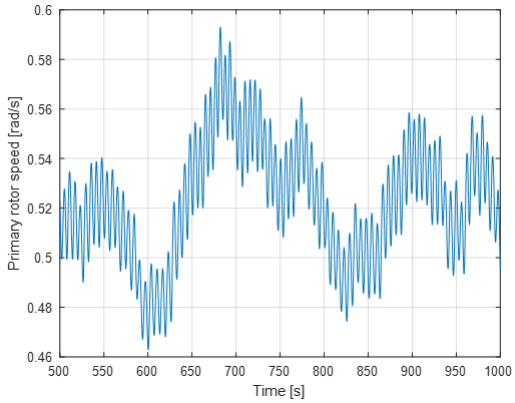

Figure 10: Primary rotor speed at 8m/s wind speed

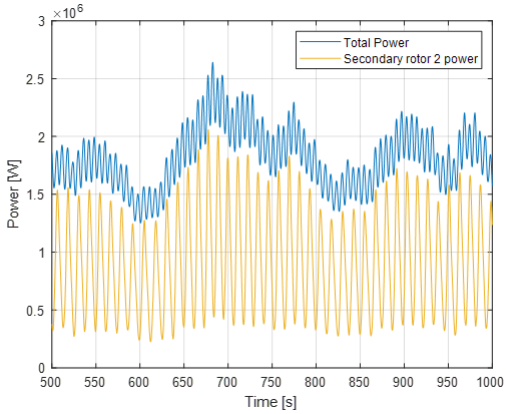

Figure 11: X-Rotor turbine power comparison

speed is held by the maximum tip speed ratio, see Figure 9. The primary rotor also holds its maximum tip speed ratio to maintain a balanced operation, see Figure 10. Figure 11 shows the power generated by one of the secondary rotors and the overall power of the turbine. As shown the secondary rotors sees large excursions of generated power as induced wind speed increases. At above rated operation, the pitch controller of the primary rotor regulates the primary rotor speed at its rated value, see Figure 12. The secondary rotors speed is balanced as a function of the primary rotor speed and the power excursions due to the high induced wind speed is limited to avoid saturation in the generator power converter. The 2p rotational sampling induced by the primary rotor is filtered out from the primary rotor rotational speed to reduced the pitch activity and fatigue loads. The primary rotor speed spectral density is shown in Figure 13.

5. Conclusions

The design of a full envelope controller to regulate the operation of the X-rotor wind turbine concept is presented. To track the desired operational strategy the controller uses a pitch controller, a pre-emptive pitching strategy and a tip speed ratio tracking controller. The

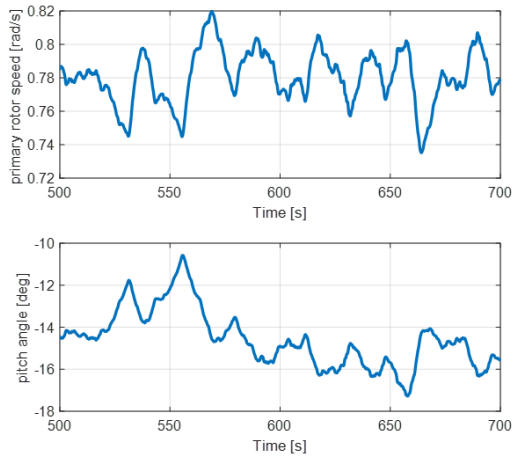

Figure 12: Primary rotor speed and pitch angle at 16m/s wind speed

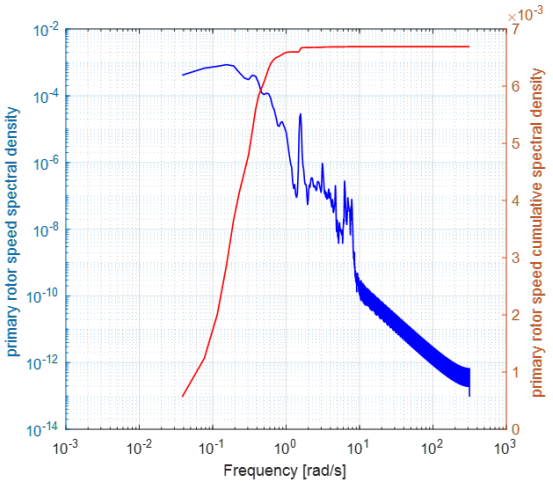

Figure 13: Primary rotor speed spectral density

operational strategy is improved by tracking an estimate of the secondary rotor torque. The balance between the primary aerdynamic torque and the secondary rotor thrust is keep in all modes of operation. In the event of a misbalance due to errors in the assumed aerodynamic characteristics, the turbine states would themselves find a more appropriate equilibrium operating point to recover the balance.

6. Acknowledgements

The authors would like to acknowledge the EU H2020 XROTOR Project 101007135 and the EP/S023801/1 EPSRC Centre for Doctoral Training in Wind and Marine Energy Systems and Structures for funding this research.

References

[1] Leithead W, Camciuc A, Amiri A K and Carroll J 2019 *Journal of Physics: Conference Series* **1356** 012031 URL `https://dx.doi.org/10.1088/1742-6596/1356/1/012031`
[2] McMorland J, Flannigan C, Carroll J, Collu M, McMillan D, Leithead W and Coraddu A 2022 *Renewable and Sustainable Energy Reviews* **165** 112581 ISSN 18790690 URL `https://doi.org/10.1016/j.rser.2022.112581`
[3] Flannigan C, Carroll J and Leithead W 2022 *Journal of Physics: Conference Series* **2265** ISSN 17426596
[4] Morgan L and Leithead W 2022 *Journal of Physics: Conference Series* **2257** ISSN 17426596
[5] Bensason D, Sciacchitano A and Ferreira C 2023 *Journal of Physics: Conference Series* **2505** ISSN 17426596
[6] Morgan L 2021 X-Rotor concept development second year report Tech. Rep. October 2021 University of Strathclyde
[7] Yen J and Ahmed N A 2013 **114** 12–17
[8] Chen L, Yang Y, Gao Y, Gao Z, Guo Y and Sun L 2019 **195**
[9] Morgan L, Stock A and Leithead W 2022 X-Rotor control simulation model Tech. Rep. March 2022 University of Strathclyde URL `https://xrotor-project.eu.`
[10] Leithead W and Connor B 2000 *Int J Control* **73** 1173–1188